Using the resonance hairpin probe and pulsed photo-detachment technique as a diagnostic for negative ions in oxygen plasma

J Conway[1], N Sirse[1], S K Karkari[1,2] and M M Turner[1].

[1]National Centre for Plasma Science and Technology, Dublin City university, Glasnevin, Dublin-9, Republic of Ireland.
[2]Institute for Plasma Research, Bhat Gandhinagar, Gujarat, India, Pin-382428

E-mail: jim.conway@dcu.ie

Abstract
In this work the resonance hairpin probe technique has been used for detection of photoelectrons generated during photodetachment experiments performed to determine negative ion density in an inductively coupled oxygen plasma. An investigation of the temporal development of the photoelectron population was recorded with the hairpin probe located inside the laser beam region and at various points outside the beam. Varying the external microwave frequency used to drive the probe resonator allowed the local increase in electron density resulting from photoelectrons to be determined. At a fixed probe frequency, we observed two resonance peaks in the photodetachment signal as the photoelectron density evolved as a function of time. Inside the laser beam the resonance peaks were asymmetric, the first peak rising sharply as compared with the second peak. Outside the laser beam region the peaks were symmetric. As the external frequency was tuned the resonance peaks merge at the maximum electron density. The resonance peak corresponding to maximum density outside the beam occurs at a delay of typically 1-2 µs as compared with the centre of the beam allowing an estimate of the negative ion velocity. Using this method, negative ion densities were measured under a range of operating conditions inside and outside the beam.

1. Introduction

Advances in plasma technologies in the area of reactive ion etching and deposition on silicon have revolutionized the latest microprocessor devices fabricated through a series of plasma processes. For nano-scale device fabrication, reactive gas mixtures such as fluorine, chlorine and hydrogen are routinely used while oxygen is necessary for side-wall surface passivation which prevents isotropic etching via the formation of dielectric oxide layers inside the microscopic etch trenches on the silicon substrates. Typical plasmas used in reactive ion etch contain electronegative gases which have a strong tendency to form negative ions whose presence give rise to a new equilibrium among the electrons and positive ion species in the plasma.

The negative ions are generated in the bulk plasma by dissociative attachment or charge transfer [1]. However, surface processes can also become important for negative ion production [2]. Surface conversion involves the interaction of neutrals and ions with a surface in a manner that results in desorption of negative ions from the surface [3, 4]. Surface convertors involving the use of low work function materials and insulating materials have been investigated [5]. Also in low pressure plasma positive ions accelerated across the plasma sheath can undergo energetic collisions near the surface creating other particles resulting in unique sheath chemistry. Negative ions are possible products of ion sheath reactions for low pressure plasmas. Negative ions generated at or near surfaces in low pressure plasmas result

in the presence of energetic negative ions in the bulk plasma as the negative ions are accelerated from the surface back into the bulk plasma across the sheath voltage and so have energies much larger than typical negative ion energies in the bulk plasma. The presence of negative ions has a major impact on the transport phenomenon of plasma species to the chamber walls which opens up an exciting area for plasma physics studies. Negative ions are also useful for the production of neutral hydrogen beams for plasma heating in fusion reactors [6, 7].

The measurement of negative ion densities in electronegative plasmas is important as they can significantly influence the plasma potential, the charge balance and the net emission from the plasma. They also play a major role in the stability of the discharge. The negative ion density can exceed the electron density and the negative ions are the main component in transport and significantly influence reaction rates for such plasmas. Many techniques have been developed that allow the application of the Langmuir probe for direct detection of negative ion density including taking the second derivative of the probe characteristic with the Druyvesteyn method modified for negative ions [8, 9, 10], comparing the ratio of saturation current of positive ions to electrons in a noble gas plasma to that in an electronegative plasma or estimating the reduction rate of electron saturation current [11, 12]. This method involves knowing the ion mass to a high degree of accuracy. However, in plasma with complex gas chemistries the typical ion mass is an aggregate of small molecular fragments which makes analysis of the ion flux to the probe complicated. Other techniques for negative ion detection using the Langmuir probe have been developed [13, 14] but these are based on highly complex probe theories. In strongly magnetized plasmas the interpretation of the electron flux to the probe is again an intricate problem [15]. Other electrical probe techniques have been developed to determine the negative ion fraction in plasmas. One such two-probe technique involves using a guarded planar probe to measure the Bohm velocity as modified by negative ions while a cylindrical probe is used to measure the electron thermal current. The ratio of these currents can then be used to determine the negative concentration in the plasma. In this paper a second technique to determine the electronegativity by looking at the difference between the plasma potential and floating potential in the plasma was also reported [16].

Optical methods have also been developed to measure absolute negative ion densities the most prominent being Cavity ring-down spectroscopy [17]. CRD requires a laser pulse to pass up and down the plasma chamber via the use of highly reflecting mirrors located at each end of the chamber to create an optical cavity and so significantly increase the optical path length of the laser pulse through the plasma and the decay of the laser light escaping through one end of the cavity after each pass of the laser pulse through the plasma chamber is recorded. The time constant associated with exponential decay in the laser energy escaping the cavity is determined. By comparing the CRD signals with plasma on and plasma off the absolute negative ion density can be measured. However there are problems associated with this technique. The cavity mirrors must be precisely aligned and reflecting. In typical plasma tools the interaction between the plasma and the mirrors often affects the reflectivity of the mirrors via deposition or etching at the mirror surfaces. In oxygen, Argon and hydrogen plasma a drift in the decay time has been reported due to water vapour affecting the mirrors and the plasma must be operated for a prolonged period before a CRD experiment can be performed to allow the system to stabilise [18]. Another problem is that this method only allows a line averaged density measurement whereas the negative ion density varies spatially within the plasma and local density variations are not considered in the results obtained with this method. Laser Thomson scattering has also been used to measure negative ion density in plasma [19]. The quality of the results obtained were compared with those obtained using Langmuir probes and found to be similar [20].

Several experimental techniques based on laser photodetachment have been developed to detect negative ion density. In this method, electrons are photodetached from negative ions using a pulsed laser beam of suitable energy and diameter, and the instantaneous increase in

electron density is recorded. Traditionally, the most common method for photoelectron detection seems to involve using a Langmuir probe placed directly in the beam path and recording the increase in saturation current following photodetachment [21, 22, 23]. Although there are problems associated with this technique it has been widely used in magnetized plasma to measure the negative ion density. Other methods used to measure the photoelectron number density include microwave interferometry [24], far-infrared (FIR) laser interferometry [25] and microwave cavity resonance [1]. However, there are problems associated with the application of each of these techniques [26].

In this experiment an investigation of negative ion densities in an inductively coupled plasma (ICP) plasma source (BARIS) operated at 13.56 MHz is investigated in the low pressure regime. Laser photodetachment and subsequent photoelectron detection with a hairpin probe is performed systematically. The two main negative ion species present in such plasmas are O_2^- and O^-. Optical photodetachment via laser irradiation is used to remove the extra electron from the negative species and the local increase in electron density is then detected using the floating resonance hairpin probe technique. When operating in the saturation region for photodetachment the increased electron density generated by photodetachment can be directly related to the negative ion densities at that region of the plasma.

2. Experimental setup.

2.1. Plasma chamber.
The BARIS (BAsic Radiofrequency Ion Source) chamber which is used for these experiments has been previously described [27, 28]. It is a stainless steel cylindrical chamber 80 cm long with an internal radius of 10 cm. Gas is flowed into the chamber using STEC SEC-4000 Series Mass Flow Controller and the chamber is pumped using a Pfeiffer Balzars turbomolecular pump which is backed by an Edwards rotary pump.

An 11 turn helical antenna of diameter 3 cm made from 1/8 inch diameter gold plated copper tubing is mounted into the chamber region through one of the chamber end walls along the chamber axis. The antenna is isolated from the vacuum chamber by a Quartz tube (i.e. re-entrant configuration). The antenna is driven by a 13.56 MHz ENI ACG10B signal generator via a standard 'L' RFPP AM20 impedance matching unit. The antenna is water cooled to allow powers of up to 1 kW to drive the system without excessive heating of the antenna. To allow access to the chamber for detachment experiments a number of viewports are included in the chamber design. A 2 cm by 6 cm wide Pyrex viewport is fitted into the antenna end wall of the chamber. This viewport extends radially from the edge of the antenna out towards the flange edge. This window is mounted at the Brewster angle to minimise laser light reflections back into the chamber. The opposite end of the chamber is sealed with a 15mm thick Pyrex viewport allowing the laser beam to enter the chamber at any position. The laser enters the chamber through the front viewport and exits the chamber via the Brewster window beside the antenna.

The hairpin probe is mounted onto the sidewall of the chamber via a Wilson seal in the antenna region of the chamber. The position of the probe can be adjusted radially using a micrometer actuator that is coupled to the probe via the Wilson seal to allow electron and negative ion density measurement at different positions across the chamber i.e. between the antenna and chamber wall. The hairpin resonator is orientated at an angle to the laser beam so that the tip of the probe can be positioned at the centre of the laser beam. Using the linear actuator system the probe can be withdrawn from the beam region and the effect on the photodetachment signal recorded at different positions.
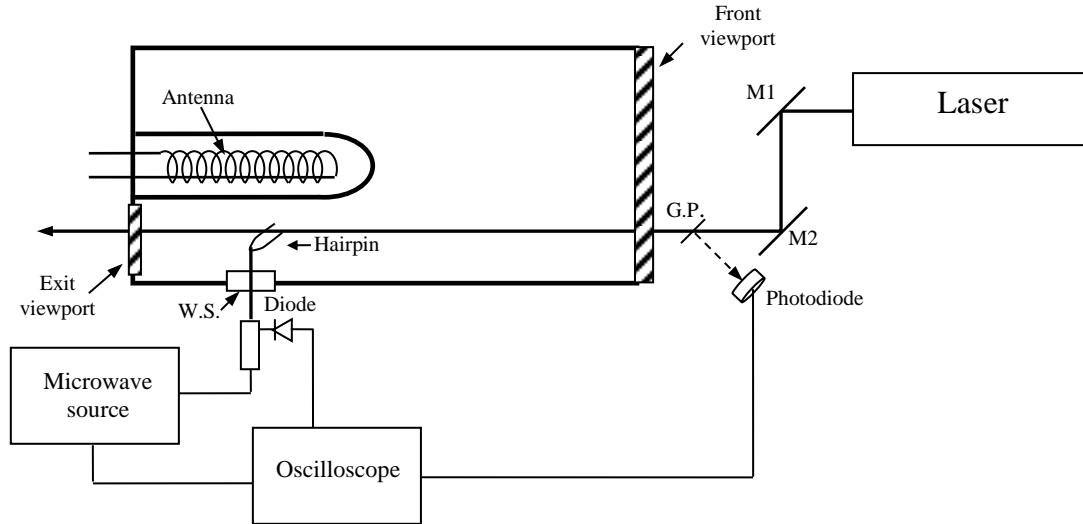
Figure 1: Schematic diagram of the experimental set-up to detect negative ion density using laser photodetachment with a floating hairpin probe. M1 and M2 - steering mirrors, G.P - glass plate, W.S - Wilson seal.

2.2. *Photodetachment and the Hair Pin Probe technique*

The laser used in this experiment is an Innolas Spitlight 600 Nd:YAG laser which has a bandwidth of < 0.03 cm^{-1} operated at a frequency of 10 Hz. The second harmonic of the laser is generated using a temperature controlled type II KTP crystal. The resulting mixture of infrared and green light is then fed into a harmonic separation assembly composed of two dichroic mirrors that transmit infrared but reflect green light. The green light at 532 nm is reflected to a series of mirrors that steer the beam to the laser exit aperture. The exit beam which has a 6 mm diameter is steered using mirrors into the plasma chamber through a quartz window and passes down the axis of the chamber parallel to the RF antenna to a quartz exit port located at the far end of the chamber. A small sheet of glass is used to reflect part of the laser beam onto a Thorlabs Det210 fast photodiode that is used to trigger the oscilloscope.

The second harmonic laser pulse at a wavelength of 532 nm introduces photons of energy 2.33 eV into the plasma region. The photon energy is insufficient to cause photodissociation (5.12 eV) or ionisation of the O_2 ($E_{iz} = 12.07$ eV) and O ($E_{iz} = 13.6$ eV) species lying in the beam path [29]. However, it is large enough to detach electrons from negative ions species, the two main negative ions in an oxygen plasma being O_2^- ($E_d = 0.44$ eV) and O^- ($E_d = 1.46$ eV). The only influence the laser beam has on the plasma composition is the removal of the extra electron from negative ions that lie in the beam path. During photodetachment, the photons interact with the negative ions and remove the attached electrons via reactions of the form $A^- + h\nu \rightarrow A + e^-$. The photoelectrons generated have energies of 0.87 eV (O^-) and 1.9 eV (O_2^-) corresponding to the difference between the photon energy and the detachment energy of the particular species [30]. The resulting increase in the electron density in the beam region causes an increase in the local dielectric constant in the plasma which can be detected using the floating hairpin probe technique.

The floating hairpin probe technique has been described previously [31]. A hairpin probe is constructed by folding a piece of wire into the shape of a hairpin which acts as a microwave resonant structure. The resonant frequency of the hairpin structure depends on the length L of the pins and the dielectric constant ε of the medium in which the hairpin is immersed, and is given by:

4

$$f_r = \frac{c}{4L\sqrt{\varepsilon}} \qquad\qquad (1)$$

where c is the speed of light. In vacuum $\varepsilon = 1$ and the vacuum resonance frequency f_o is c/4L. For weakly magnetized plasma, the dielectric constant is given by:

$$\varepsilon = 1 - \frac{\omega_p^2}{\omega^2} \qquad\qquad (2)$$

where ω_p is the electron plasma frequency.

Using the two expressions above the electron density n_e in the plasma can be written as:

$$n_e = \frac{f_r^{\;2} - f_0^{\;2}}{0.81} \; (10^{10} \text{ cm}^{-3}) \qquad\qquad (3)$$

where f_r and f_0 are in GHz.

In this experiment the hairpin probe is driven by a Hewlett Packard HP8350 microwave generator with a sweep range from 1 GHz to 8.0 GHz. Typically the microwave frequency is varied between 2.0 – 4.0 GHz and a directional coupler connected between the output of the microwave source and the 50 Ω coaxial line whose extreme end is terminated by a single turn loop antenna measures the reflected power from the terminated end. The magnitude of the reflected signal which varies with frequency is converted into a negative dc output using a Schottkey diode and captured on an oscilloscope (Tektronix TDS3034B 300 MHz). At the resonance frequency, maximum power is coupled into the hairpin resulting in a sharp drop in the reflected signal. Correspondingly the output signal from the diode drops almost to zero at the resonant frequency allowing f_r to be obtained precisely.

During the photodetachment process electrons are instantaneously detached from negative ions lying in the laser beam path resulting in a sharp rise in electron density along the beam path which then decays at a rate determined by negative ions diffusion from the adjacent plasma layer to replenish the annihilated negative ions in the beam region [32]. The bulk negative ion density n_- can be determined by subtracting the background electron density from the peak photoelectron density.

To obtain the time-resolved electron density peak, we apply a specific frequency to the hairpin and we look at the reflected signal from the diode as a function of time. When the applied frequency is off resonance the output voltage from the diode measures a steady state negative dc voltage output. As the frequency is tuned in within the range of the time-varying plasma frequency ω_p (or n_e) the time dependent plasma permittivity given by (2) satisfies the resonance condition with the applied frequency during specific times. The resonance condition is identified by observing a relative drop in the reflected signal amplitude with respect to the off resonance reflected signal.

3. Results and discussion
The negative ion density was investigated both inside and outside the laser beam region by varying the position of the probe in relation to the laser beam to determine the effect on the negative ion density detected by the hairpin probe. Measurement of negative ion density in the plasma involves firstly aligning the laser so that it passes through the chamber viewports and plasma at the desired radial position in the chamber. The hairpin probe is then positioned using the linear actuator system so that the probe tip is located at the laser beam centre. The background electron density in the plasma is determined by adjusting the microwave frequency driving the hairpin till a resonance condition is established between the hairpin

resonator and the surrounding plasma and the driving frequency of the microwave generator is left at this value. The laser is then fired and a fast photodiode picks up part of the beam and sends a trigger pulse to the oscilloscope to synchronize the hairpin signal with the laser pulse. The increase in local electron density due to the photodetachment process alters the plasma frequency and so the dielectric constant around the probe shifting the plasma and hairpin off resonance. The photoelectron density at the hairpin varies over time as a pulse and the resulting signal has a distinctive signature corresponding to the electron density first increasing above the background resonant frequency (2.12 GHz) as the newly generated photoelectrons arrive at the probe, and then dropping back to the background resonant frequency as the photoelectrons travel into the surrounding plasma region and the pulse dies away. Therefore, at 2.12 GHz frequency, the probe remains off resonance over a substantial period of time (approximately 1-2 μs) as the photoelectrons diffuse through the probe region, and it displays maximum negative voltage output from the diode as shown in figure 2 and figure 3 below. The plots corresponding to other frequencies have been shifted in scale such that the amplitude of the reflected signal prior to the injection of the laser beam is set to zero.

As the hairpin frequency is gradually increased to bring the probe back to a resonance with the increased plasma frequency resulting from the enhanced electron density in the plasma caused by photodetachment we observe that two distinct peaks begin to emerge in the trace recorded on the oscilloscope as can be seen in figure 2 and figure 3 below.
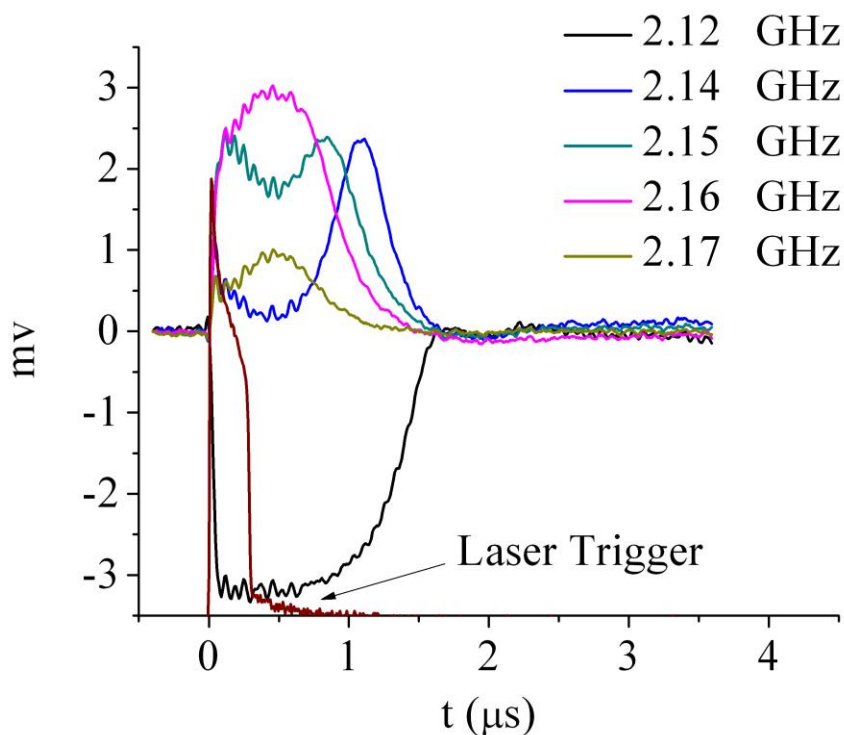

Figure 2: Reflected signal obtained from the Schottkey diode corresponding to different tuning frequency as function of time. All signals have been scaled to reduce the dc amplitude to zero prior to the laser pulse. The signal corresponding to 2.12 GHz is the resonant frequency of the background plasma (t < 0 s). At a greater frequency than the background resonance, the spectrum of the waveforms show two peaks which satisfy the same resonance conditions during the evolution in electron density as the density increase and fall to the background level following the photo-detachment. At the frequency corresponding to the maximum density only one peak is possible.

The first peak correspond to the increasing plasma frequency resulting from the rising electron density bringing the plasma back to resonance with the increased probe frequency as the photoelectron pulse grows while the second peak corresponds to a resonance condition again being reached as the electron density dies back down. As the microwave frequency

driving the hairpin probe increases the two peaks move closer together as the probe is gradually brought to resonance with the surrounding plasma following photodetachment and when the hairpin driving frequency reaches resonance with the photodetached plasma electron density the two peaks merge into a single peak in the oscilloscope trace as shown in figure 2 and figure 3.

Assuming plasma quasineutrality is maintained during the complete process, the peak electron density n_e(peak) must correspond to the magnitude of the positive ion density (n_+) inside the beam column which is assumed to be unperturbed by the process of photo-detachment. By subtracting the electron density prior to the injection of the laser pulse from n_e(peak) ~ n_+, it is hence possible to estimate the negative ion density.

Using this approach the negative ion density is calculated at different positions relative to the laser beam by moving the hairpin in 1mm steps outside the beam region and repeating the photodetachment experiment at each position. The signal recorded outside the beam was observed to have different characteristics to the signal inside the beam. The peaks observed in the signal inside the beam region are asymmetrical and only become symmetric at frequencies close to the resonance condition as can be seen in figure 2, while the resonance peaks observed outside the laser beam are symmetrical at all probe frequencies up to the resonance frequency as shown in figure 3.
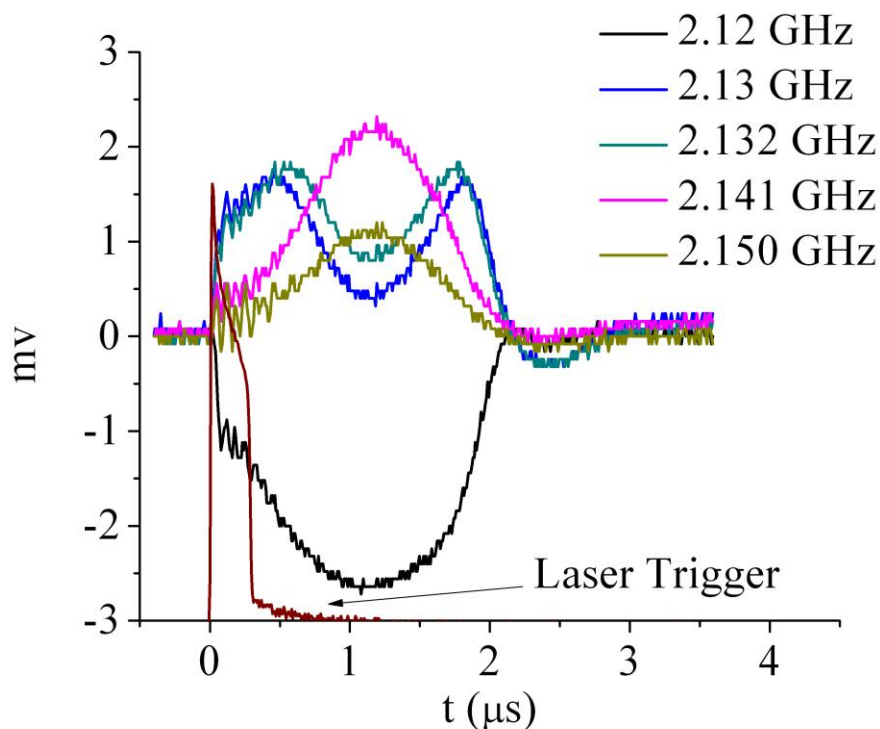

Figure 3: Hairpin signals recorded outside the laser beam as the probe is tuned to the plasma electron density following photodetachment. At 2.12 GHz there is a dip due to the photoelectron population shifting the probe and plasma off resonance. At higher frequencies two symmetrical resonance peaks appear corresponding to the electron density matching the frequency of the hairpin probe firstly as the electron density increases and again as the electron density decays. As the hairpin resonator frequency is shifted toward the new plasma frequency following photodetachment the two peaks gradually merge to produce a single maximum when the resonator is tuned to the electron density at 2.141 GHz. At higher frequencies the amplitude of the signal drops as the probe is moved off resonance.

The asymmetry inside the beam region is attributed to the response time of the probe. The generation of photoelectrons in the beam region is almost instantaneous following passage of the laser pulse through the plasma and the probe does not have a sufficiently fast rise time to

fully respond to the increasing electron density resulting in little to no resonance peak appearing in the signal as the electron density rapidly increases. However the decay time for the electron density which corresponds to photoelectrons diffusing from the beam region is much slower as this is determined by the timescale over which the negative ions diffuse back into the beam region. The analytical solution for the flow of negative ions into the beam region is given by the expression:

$$n_-\left(r=0,t\right)=n_0\exp\left(-\left(R/v_{th}^-t\right)^2\right) \tag{4}$$

where r is the distance from the laser beam centre, R is the beam radius, v_{th}^- is the negative ion thermal velocity [32]. Quasineutrality considerations ensure that the excess electrons leave the beam region at a rate determined by the negative ion thermal velocity.

Thus the photoelectrons escape from the beam region over a timescale of microseconds which is sufficiently slow to allow the probe to respond to the changing electron density resulting in a significantly stronger resonance peak in the signal as the photoelectron pulse dies away. Outside the beam region the dynamics of the photoelectron pulse is determined by the negative ion diffusion into the beam region. As a result both the rate of increase and the rate of decrease of the electron density outside the beam are sufficiently slow to allow the probe to react resulting in two strong resonant peaks appearing in the signal.

The increase in local electron density detected by the probe will correspond exactly to the negative ion density prior to photodetachment provided the system is operated at saturation (100 % photodetachment). The laser flux needs to be sufficiently high so that the photon density in the beam is adequate to detach electrons from all the negative ions in the beam region. The detachment fraction of negative ions is given by the expression [19]:

$$\frac{n_-^{detached}}{n_-}=1-\exp\left(\frac{-\sigma}{hv}\frac{E}{A}\right) \tag{5}$$

where E is the energy of the laser beam, σ is the photodetachment cross section, v is the laser frequency and A is the beam cross section area. By varying E and A the laser power can be adjusted to ensure saturation level for the experiment. With a laser beam diameter of 6mm, measurements of n_e after the laser was fired were recorded with the hairpin probe to detect the photoelectron enhanced density as laser power was increased. The laser energy was monitored using a Molectron PowerMax 500A laser power meter fitted with a PM10V1 power probe.

The hairpin probe was initially positioned at the centre of the laser beam and the negative ion density measured as a function of laser power using the hairpin probe technique. The results are plotted in figure 4 along with the theoretical curve generated using equation (5). From the figure it is seen that above a laser flux of 200 mJ/cm^2 the recorded signal begins to exceed the theoretical curve. This deviation may be attributed to laser ablation effects at the probe. Such problems can be significantly higher in the case of deposition plasmas as has been reported by previous workers using Langmuir probes [22, 23]. In such a situation, the techniques such as the eclipse method have been developed to try and overcome this problem [23]. The size and shape of the hairpin resonator as compared with a single Langmuir probe make shadowing of the probe unrealistic or rather difficult. In this work the hairpin probe was placed outside the beam area to avoid ablation as has been suggested in previous work [33] which found that the peak of the perturbed electron density travels out from the beam region with the ion acoustic velocity and the maximum of the pulse decreases inversely proportional to the distance from the beam center. This suggests that locating the probe outside the beam region will result in an underestimated value of the negative ion density being recorded. Hence our primary aim

was to evaluate the difference if the probe is situated outside the beam with respect to the beam centre.
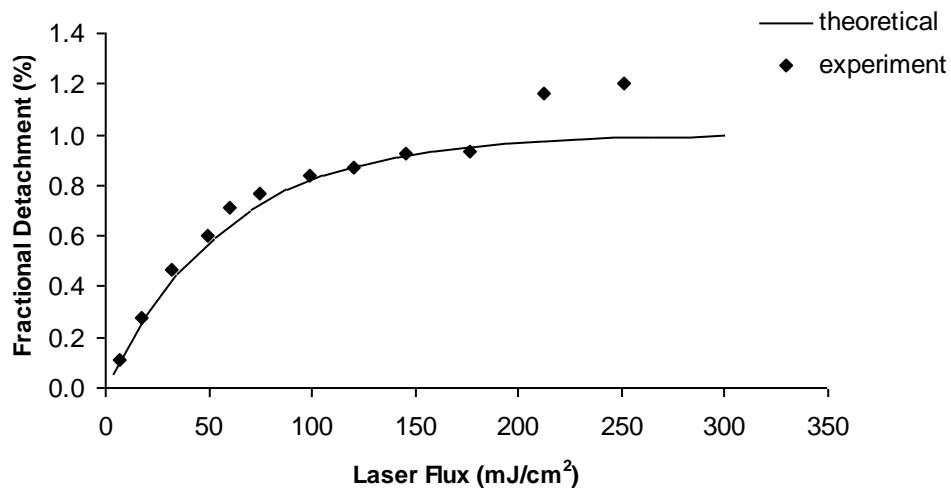

Figure 4: Plot of photodetachment fraction as a function of laser energy density at 532 nm with the probe placed inside the beam area. The operating conditions of the plasma are 30 mTorr and 200 W RF power.

To determine the decrease in n_- recorded as a result of locating the probe outside the beam region probe measurements were recorded as a function of distance from the beam centre at several laser powers below the ablation threshold and the data normalized for each laser power and plotted below in figure 5. The probe was first placed at the beam centre and the negative ion density recorded. The probe was moved in one mm increments out from the beam centre using the micrometer actuator coupled to the probe, and n_- was recorded at each position. This was repeated for various laser powers and the resulting data is shown in figure 5. The relative change in the negative ion density signal as the probe moves from inside the beam to outside appears to be independent of laser power as the three normalized plots in figure 5 seem to overlap each other well indicating the laser power does not affect the relative size of the signal variation with position recorded.
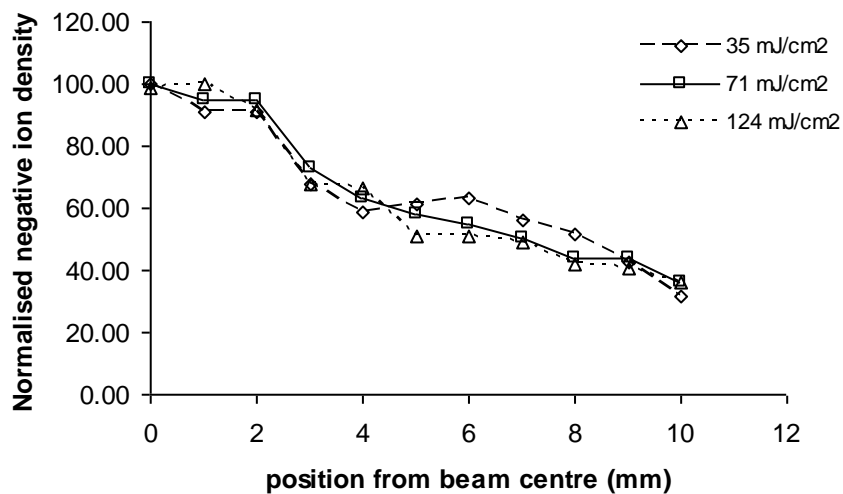

Figure 5: Hairpin probe data recorded at various positions moving from the beam centre outwards. These measurements were performed at reduced laser powers to avoid ablation effects. The data is normalized for each laser power.

The results suggest that at the higher laser powers required for saturation of the detachment signal, the relative change between the beam interior and exterior at various positions should also be the same allowing n_- to be determined with the probe placed outside the beam region while avoiding ablation of the probe. The laser beam has a diameter of 6 mm while the separation between the pins is 4 mm. As the probe was moved from inside the beam to outside there was a sharp decrease in the measured density at the 3mm region to ≈ 65 % the density measured inside the beam corresponding to the probe moving outside the laser beam. However the density signal then remains fairly constant as the probe is moved further out over a 3mm to 6mm distance from the beam centre before starting to drop once again. This behavior enables us to correct the data recorded outside the beam region to correspond to the actual negative ion density inside the beam. When operating at laser saturation with the probe placed outside the beam the recorded negative ion densities can be corrected to get the true negative ion density in the plasma.

The probe was set at a distance of 4 mm from the beam centre and a saturation curve was again recorded at this point. The resulting data is plotted along with the theoretical curve using equation (5) in figure 6. From the figure saturation of the negative ion density signal occurred above laser energy densities of 200 mJ/cm^2 per pulse. No ablation effects were recorded at this position. For the purpose of the measurements performed in this experiment the laser flux was set at 220 mJ/cm^2 unless otherwise stated.
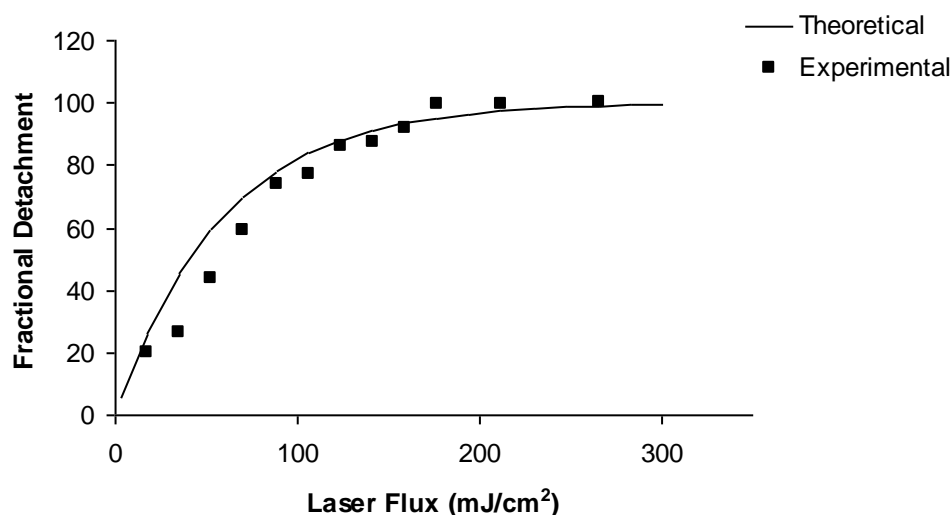

Figure 6: Plot of photodetachment fraction as a function of laser energy density at 532 nm. The operating conditions of the plasma are 30 mTorr and 200 W RF power.

Using this approach, the hairpin probe photodetachment technique was applied to measure negative ion densities in an oxygen ICP over a range of RF powers. The results are presented below.

3.1 Effects of RF power.
In figures 7 and 8, the electron density and the negative ion density plots in an oxygen inductive plasma are obtained as a function of the RF power into the chamber. The RF power was varied between 50 W and 500 W while keeping the pressure constant at 30 mTorr and a flow rate of 100 sccm.
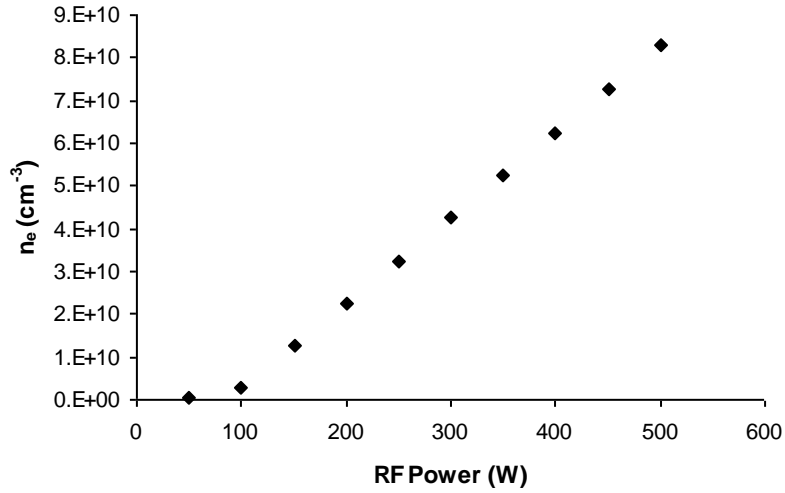
10

Figure 7: Variation in electron density verses RF power in an oxygen plasma operating at 30 mTorr and 200 sccm.
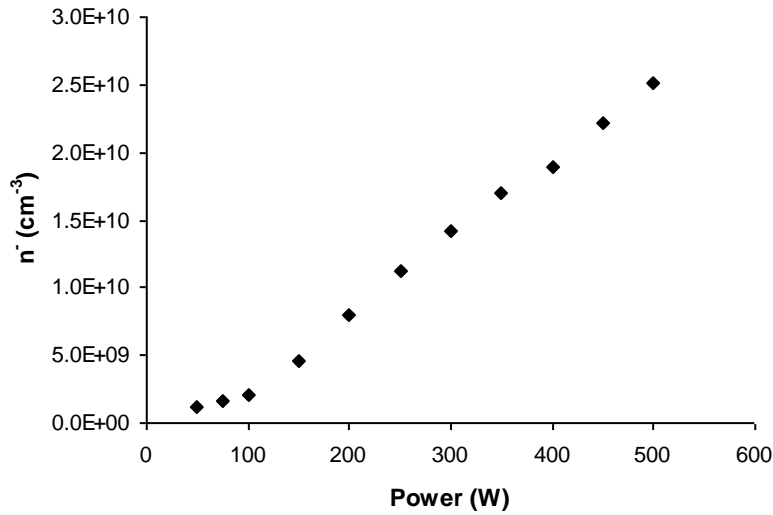

Figure 8: Variation in negative ion density verses RF power (on beam) in an oxygen plasma operating at 30 mTorr and 200 sccm.

As expected the electron density in figure 7 increases almost linearly with increasing RF power for powers above 100 W. The linear relationship between the applied power and density suggests that the net electron density of the plasma n_o is below the critical limit at which the absorbed power, $P_{abs} \propto n_o I_{rf}^2$ or $n_o = \dfrac{P_{abs}}{e u_B A_{eff} E_T}$ [34].The production of negative ions is primarily governed by dissociative attachment: $e + O_2 \rightarrow (O_2)^* \rightarrow O^- + O$. In our experiments the negative ion density in figure 8 increases in a linear manner in line with the increasing electron density with the rf power suggesting that the dissociative attachment is the dominant process for the production of negative ions in this case. The electronegativity of the plasma is plotted in figure 9. At low powers below 100 W, the negative ion fraction is found to be higher than the electron density with $\alpha = n_-/n_e \sim 1.5$ whereas α drops significantly to about 0.3 with increasing power (or n_e). This is consistent with the fact that electron density increases at a higher rate than negative ion density with increasing RF power. This suggests that negative ion destruction mechanisms become increasingly prominent as the RF power

11

increases up to 150 W. The main destruction channels for negative ions are electron detachment and ion-ion neutralization via the reactions $e + O^- \rightarrow O$ and $O^- + O_2^+ \rightarrow O + O_2$. From figure 7 the electron density in the plasma increases with increasing RF power which would result in an increased rate of destruction of negative ion which is consistent with our findings. Above 150 W α remains essentially constant indicating that an equilibrium is reached between the production and destruction rate of the negative ions as the electron density further increases with increasing RF power, provided the electron temperature remains constant. As the measurements were performed at constant pressure the electron temperature T_e remains essentially constant over the RF power range and has been measured previously for the system to be ~ 4 eV using a Langmuir probe.
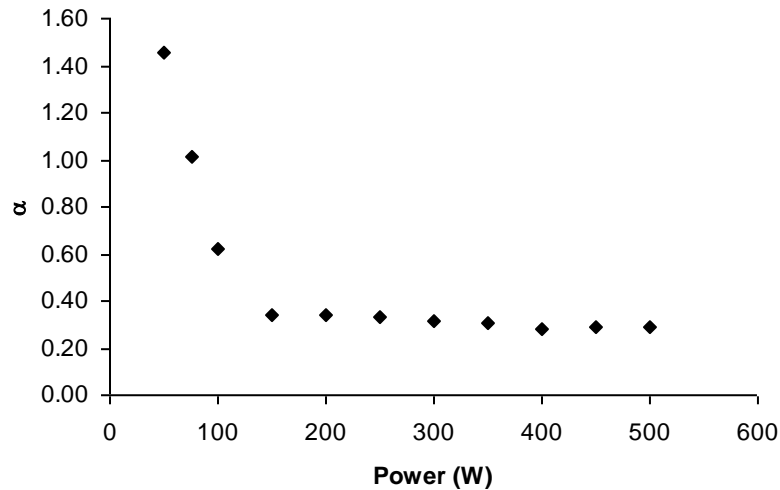

Figure 9: Plot of ratio of negative ion density to electron density verses RF power (on-beam) in an oxygen plasma operating at 30 mTorr and 200 sccm.

The negative ion velocity was also determined by considering the time delay between the photoelectron peak inside and outside the beam. The peak signals at the beam centre and at a distance of 6 mm outside the beam were recorded and are displayed in figure 10 below. From the off-beam peak the time for the photoelectrons to leave the beam zone and arrive at the probe is 1.19 μs. As the electron velocity leaving the beam zone is determined by the negative ion velocity entering the beam region this allows the negative ion velocity to be determined as 5×10^3 m/s for a pressure of 30 mTorr and 200W RF power. This is typically one order of magnitude greater than the neutral gas thermal speeds in the plasma. This large velocity can be attributed to the fact that negative ions generated near the plasma extremities are accelerated by the large potential in these regions back into the plasma where they relax back to the gas temperature by collision processes. However at lower pressures the relaxation process can take longer than the negative ion lifetime resulting in the larger negative ion velocities observed relative to the neutral gas speeds. Also, negative ions can initially have large energies when they are first created in the attachment process which would also account for this.
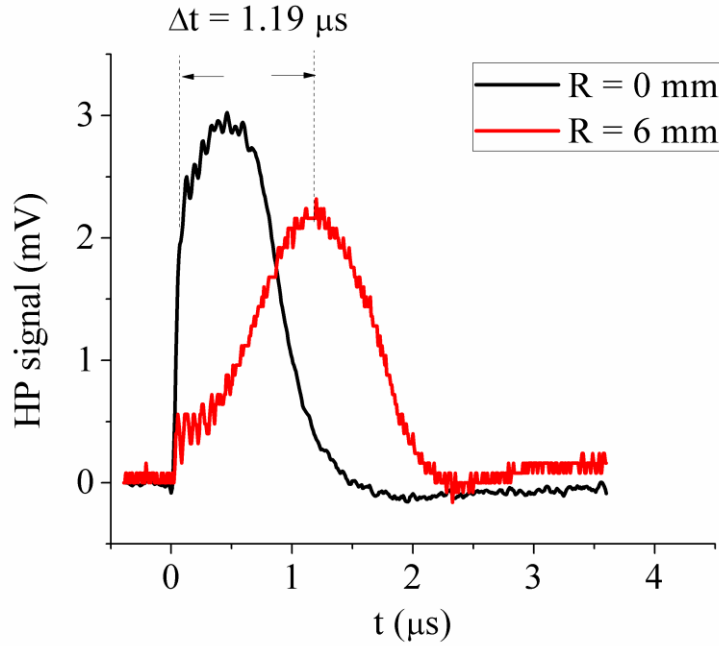
Figure 10: Probe resonant signal for the peak electron density at the beam centre and at a radial distance of 6 mm from the centre.

4. Conclusion.

In this paper we have successfully recorded the negative ion density in an oxygen plasma using photodetachment in conjunction with the floating hairpin probe method. The signal characteristics observed have been explained in terms of the dynamics of the photoelectron population and the probe response time. Ablation effects were found to be negligible unlike the case where Langmuir probes are used as the probe is insensitive to small changes in the density. However such effects are substantial in the case of Langmuir probes as the probe tip which is biased at a positive potential with respect to the plasma can arc leading to spurious electron current.

The negative ion density was recorded as a function of RF power and was found to increase in a manner determined by the increase in electron density. The electronegativity of the plasma was found to drop significantly with increasing power as the rate of increase of n_- is smaller than the rate of increase of n_e. Effects of measuring the negative ion density with the probe located outside the beam were investigated and indicate that in plasma such as deposition plasma where ablation could present a serious barrier to accurately determining the absolute negative ion density placing the probe outside the beam would still allow n_- to be determined once the correction factor required to compensate for the drop in signal measured away from the beam centre was measured. The position of the photodetachment electron density peak along the beam centre and outside the beam was used to obtain a qualitative estimate of negative ion temperature.

Acknowledgements

References

[1]   Stoffels E, Stoffels W W, Vender D, Kando M, Kroesen G M W and de Hoog F J 1995 *Phys. Rev. E.* **51** (3) 2425.

[2] Stoffels E, Stoffels W W and Kroesen G M W 2001 *Plasma Sources Sci. Technol.* **10** 311.

[3] Roncin P, Borisov A G, Khemliche H, Momeni A, Mertens A and Winter H 2002 *phys. Rev. Lett.* **89** 043201.

[4] Schiesko L, Carrera M, Layet M and Cartry G 2009 *Appl. Phys. Lett.* **95** 191502

[5] Auth C, Borisov C and Winters H 1995 *Phys. Rev. Lett.* **75** 2292.

[6] Hamilton G W and Bacal M 1991 *IEEE Trans. Plasma Sci.* **19** 1143.

[7] Gutser R, Wünderlich D, Fantz U et al 2010 *Plasma Phys. Control. Fusion.* **52** 045017.

[8] Thomson J B *Proc. Phys. Soc. A* 1959 **73** 818.

[9] Vucelić M and Mijović S 1998 *J. Appl. Phys.* **84** 4731.

[10] Amemiya H 2000 *Vacuum* **58** 100.

[11] Shindo M, Uchino S, Ichiki R, Yoshimura S and Kawai Y 2001 *Rev. Sci. Instrum.* **72** 2288.

[12] Nakamura Y, Nakamura M and Itoh T 1976 *Phys. Rev. Lett.* **37** 209.

[13] Bryant P, Dyson A and Allen J 2001 *J. Phys. D: Appl. Phys.* **34** 95.

[14] Popov T K, Gateva S V 2001 *Plasma Sources Sci. Technol.* **10** 614.

[15] Gogna G S and Karkari S K 2010 *Appl. Phys. Lett.* **96** 151503

[16] Chabert P, Sheridan T E, Boswell R W and Perrin J 1999 *Plasma Sources Sci. Technol.* **8** 561.

[17] Quandt E, Kraemer I, and Döbele H F 1998 *Europhys. Lett.* **45** 32.

[18] Grangeon F, Monard C, Dorier J-L, Howling A A, Hollenstein Ch, Romanini D and Sadeghi N 1999 *Plasma Sources Sci. Technol.* **8** 448.

[19] Noguchi M, Ariga K, Hirao T, Suanpoot P, Yamagata Y, Uchino K and Muraoka K 2002 *Plasma Sources Sci. Technol.* **11** 57.

[20] Noguchi M, Hirao T, Shindo M, Sakurauchi K, Yamagata Y, Uchino K, Kawai Y and Muraoka K 2003 *Plasma Sources Sci. Technol.* **12** 403.

[21] Bacal M, Hamilton G W, Bruneteau A M, Doucet H J, and Taillet J 1979 *Rev. Sci. Instrum.* **50** 719.

[22] Dodd R, You S-D, Bryant P M, and Bradley J W 2010 *Plasma Sources Sci. Technol.* **19** 015021.

[23] Kajita S, Shinichiro K and Tanaka S 2005 *Plasma Sources Sci. Technol.* **14** 566.

[24] Hebner G A, Blain M G, Hamilton T W, Nichols C A and Jarecki R L 1999 *J. Vac. Sci. Technol. A.* **17** (6) 3172.

[25] Schiffer C and Uhlenbusch J 1995 *Plasma Sources Sci. Technol.* **4** 345.

[26] Katsch H M, Sturm T, Quandt E and Döbele H F 2000 *Plasma Sources Sci. Technol.* **9** 323.

[27] Cunge G, Crowley B, Vender D, and Turner M M 1999 *Plasma Sources Sci. Technol.* **8** 576.

[28] Cunge G, Crowley B, Vender D, and Turner M M 2001 *J. Appl. Phys.* **89** (7) 3580.

[29] Shibata M, Nakano N and Makabe T 1997 *J. Phys. D: Appl. Phys.* **30** 1219.

[30] Amemiya H and Suzuki T 1990 *Japan. J. Appl. Phys* **29** L1712.

[31] Karkari S K, Gaman C, Ellingboe A R, Swindells I and Bradley J W 2007 *Meas. Sci. Technol.* **18** 2649.

[32] Friedland L, Ciubotariu C I and Bacal M 1994 *Phys. Rev. E* **49** 4353.

[33] Nishiura M, Sasao M, Wada M and Bacal M 2001 *Phys. Rev. E.* **63** 036408.

[34] Liebermann M A and Lichtenberg A J 1994 *Principles of Plasma Discharges and Materials Processing* (New York: Wiley)